Model relation between the energy-band edge and the Fermi level of the nondegenerate semiconductor TiO$_2$: Application to electrochemistry

Guo-Ling Li (李国岭),[*] Wei-Xue Li (李微雪),[†] and Can Li (李灿)[‡]

State Key Laboratory of Catalysis, Dalian Institute of Chemical Physics, Chinese Academy of Sciences, Dalian 116023, China
(Received 14 November 2010; published 8 December 2010)

Assuming small-polaron model, an effective relation between the energy-band edge and the Fermi level is derived for the nondegenerate semiconductor. The new relation is distinct from the standard one based on rigid-ion model, and could be generally applied to electrochemistry to obtain valid band-edge positions from the measured flat-band potentials for small-polaron semiconductors. We reassign the band-edge position of small-polaronlike rutile TiO$_2$. Essence of the new model and relation, e.g., in understanding photoinduced interfacial charge transfer, is demonstrated in the comparative studies of anatase and rutile TiO$_2$ that are used in photocatalysis and dye-sensitized solar cells.

I. INTRODUCTION

The understanding of elementary excitation spectra in real materials is of fundamental and practical importance.[1,2] Electronic elementary excitations or quasiparticles, e.g., free electrons/holes, excitons, and polarons, are crucial to explain electrical, optical, magnetic, thermal, and chemical properties of semiconductors. When the rigid-ion or rigid-band approximation stands,[3] the electronic elementary excitation spectrum of a common semiconductor can often be described by the standard energy-band structure with the Fermi level E_F and the band gap E_g between the valence-band (VB) edge E_V and the conduction-band (CB) edge E_C.[2] When the rigid-ion approximation breaks down, as reported in ionic crystals such as TiO$_2$, NiO, WO$_3$, SrTiO$_3$, and KTaO$_3$, the electronic elementary excitation spectra should be described by small-polaron model instead.[3–8] It is noteworthy that, the standard energy-band structure, denoted as rigid-ion model, has been extensively applied to semiconductor-related fields such as electrochemistry, photocatalysis, and photovoltaics.[9,10] For example, the standard relations between E_F and E_C/E_V based on rigid-ion model have long been used in electrochemistry to obtain the band-edge position (BEP) from the measured flat-band potential E_{fb}, i.e., E_F of a semiconductor.[9] Once the BEP of the semiconductor is obtained, a thermodynamic prediction can be made for charge-transfer processes at the semiconductor-electrolyte or semiconductor-dye interface.[9–11]

TiO$_2$ is an important wide-band-gap semiconductor. The two common phases of TiO$_2$, i.e., anatase and rutile, are widely used in photocatalysis and dye-sensitized solar cell (DSSC). Rutile is known as a typical small-polaron semiconductor displaying the characteristic properties such as large effective mass of current carrier, low drift and Hall mobilities, and multiphonon feature of infrared-absorption spectra.[3,4] However, anatase and rutile have been practically assumed to have similar electronic elementary excitation spectra which are described either by rigid-ion model in most work or by small-polaron model in some recent work.[12] This rather confused situation may lie in the ambiguous understanding of the rigid-ionlike or small-polaronlike nature of anatase and rutile. One would suffer from the applications of

the improper models for electronic elementary excitation spectra of TiO$_2$. An indication is illustrated here with mixed anatase and rutile in which the thermodynamic requirement of charge transfer seems violated. Experiments found that the mixed-phase TiO$_2$ displays much higher photoactivity than any single one, which is attributed to the enhanced spatial charge separation in the mixture.[13,14] According to the measured E_{fb} and the standard relation, the E_C of rutile was assigned lower than that of anatase,[15] indicating that photoexcited electrons would transfer from anatase to rutile. Puzzlingly, the opposite direction of electron transfer is evidently favored by other experiments.[14] So far this dilemma of charge transfer remains in debate.[12]

In this paper, we re-examine the models for electronic elementary excitation spectra of semiconductors, and derive an effective relation between E_C and E_F for small-polaron semiconductors. We argue that the new relation rather than the standard one should be used in electrochemistry to obtain valid BEPs of small-polaron semiconductors, and discuss the physics underlying the new model and relation. As an example, we clarify the rigid-ionlike nature of anatase and small-polaronlike nature of rutile, reassign the BEP of rutile, and demonstrate the applications of the new model and relation in two comparative studies of anatase and rutile. Herein we stress that the new model and relation are crucial to thermodynamic and kinetic understandings of photoinduced charge-transfer processes at the interface of small-polaron semiconductor.

II. RESULTS AND ANALYSIS

We start with the model-dependent nature of current carriers or thermally excited quasiparticles. Unless noted otherwise, the semiconductor is referred to a nondegenerate n-type one for brevity. Figure 1(a) shows the energy-level diagram of rigid-ion model.[2] In rigid-ion model the thermally excited quasiparticle, i.e., the CB electron, locates at E_C. Figure 1(b) is the energy-level diagram of small-polaron model.[8] The small polaron is a quasiparticle composed of a self-trapped electron and a local lattice deformation accompanying the self-trapping.[3,5] It has been proved that, due to strong short-range electron-lattice couplings, an excess elec-
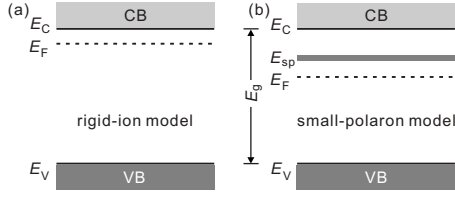
FIG. 1. Energy-level diagrams based on (a) rigid-ion model and (b) small-polaron model for a nondegenerate n-type semiconductor. Donor levels below E_F are not shown.

tron placed in a three-dimensional system has two stable states in adiabatic limit, namely, a CB electron state and a small-polaron state.[5,16] The thermally excited quasiparticle would locate at the lower-lying small-polaron band (SB) E_{sp} rather than at the higher lying E_C, in accordance with the fact that small polarons play the role of current carriers in the small-polaron semiconductor.[3–8]

We then focus on the nature of photoexcited quasiparticles. The excitonic effect is excluded for simplicity. After photoexcitation to the CB, the hot electron with excess energy relaxes rapidly to the CB edge via electron-phonon interactions.[17] In rigid-ion model the relaxed electron remains in E_C until the electron-hole recombination happens.[17] In small-polaron model the relaxed electron stays at E_C until it decays into a small polaron via electron-multiphonon interactions.[18] Additionally, the optical transition from the VB to the lattice-coupled SB is prohibited due to Franck-Condon principle.[19]

At thermal equilibrium the position of E_F relative to the energy level of thermally excited quasiparticles can, in principle, be determined by Fermi-Dirac statistics. For a nondegenerate semiconductor, Fermi-Dirac statistics approaches Maxwell-Boltzmann statistics. According to rigid-ion model in Fig. 1(a), we outline the derivation of the relation between E_C and E_F.[2,9] Maxwell-Boltzmann statistics tells that, at a given temperature T, the density of electrons which are thermally excited into CB is $n = N_C \exp[-(E_C - E_F)/k_B T]$, where $N_C = 2(2\pi m^* k_B T/h^2)^{3/2} \sim 10^{19}-10^{20}$ cm^{-3} is the effective density of states of CB, m^* the effective mass of CB electron, k_B Boltzmann's constant, and h Planck's constant. Above the ionization temperature of shallow states (~ 100 K), $n \cong N_d$, where $N_d \sim 10^{15}-10^{18}$ cm^{-3} is the density of donors. So we get the standard relation,

$$E_C = E_F + \Delta E, \tag{1}$$

where $\Delta E \cong k_B T \ln(N_C/N_d) \sim 0.1-0.3$ eV at room temperature.

Assuming small-polaron model in Fig. 1(b), we derive likewise the relation between E_{sp} and E_F,

$$E_{sp} = E_F + \Delta E'. \tag{2}$$

Here, $\Delta E' \cong k_B T \ln(N_{sp}/N_d) \sim 0.2-0.4$ eV at room temperature, $N_{sp} = 2N_0$ is the effective density of states of SB, $N_0 \cong a^{-3} \sim 10^{22}$ cm^{-3} the density of cations available as a site for small polaron, and $a \sim 4$ Å the lattice parameter.[3,6] The factor 2 in $N_{sp} = 2N_0$ arises from spin degeneracy.[6] Additionally, the small-polaron binding energy is defined as E_b

$= E_{pol} - E_{dis}$, where $E_{pol} = E_C - E_{sp}$ is the polarization energy, and E_{dis} the distortion energy of small polaron.[7,20] Thus, the effective relation between E_C and E_F can be written as

$$E_C = E_F + \Delta E' + E_b + E_{dis}. \tag{3}$$

For a nondegenerate p-type semiconductor, we obtain similar relations between E_V and E_F, i.e., $E_V = E_F - \Delta E$ in rigid-ion model, and $E_V = E_F - \Delta E' - E_b - E_{dis}$ in small-polaron model. Noting that large and intermediate polarons may exist in real materials. For a large-polaron semiconductor with the large-polaron band very close to CB,[5] Eq. (1) is a good approximation. For an intermediate-polaron semiconductor which is more small polaronlike, Eq. (3) should be considered.

Under flat-band condition the E_F of a semiconductor equals the measured E_{fb}.[9] If E_{fb} is substituted for E_F, the above relations together with $E_g = E_C - E_V$ can be generally applied to electrochemistry to obtain the positions of E_C, E_V and E_{sp} for rigid-ionlike and small-polaronlike semiconductors, respectively. We argue that the BEPs of small-polaron semiconductors misassigned according to Eq. (1) should be reassigned in terms of Eq. (3). For a small-polaron semiconductor, the position of E_C is underestimated $E_b + E_{dis} + \Delta E' - \Delta E$ by Eq. (1); if the lowest unoccupied energy level of a counter-contacted material happens to lie between the underestimated and the reassigned E_C, we would predict a wrong direction of interfacial charge transfer using the underestimated E_C. The reassignment of BEPs is therefore necessary for the thermodynamic understanding of charge transfer at the interface of small-polaron semiconductor.

The small-polaron model brings new physics into the interfacial charge-transfer processes. (1) In addition to the CB channel, the SB channel may be involved in the charge-transfer processes at the interface of small-polaron semiconductor. (2) Besides thermodynamics, kinetics is required to interpret charge transfer. A rough kinetic estimation can be made based on the typical time scales of electronic processes. In the bulk, the electron-hole recombination occurs normally on the nanosecond (ns) time scale for a direct-gap semiconductor and on the microsecond (μs) or sub-μs time scale for an indirect-gap one,[17] and the CB electron decays into a small polaron on the order of a phonon period, i.e., the picosecond (ps) or sub-ns time scale.[17,18] For a free small polaron, its lifetime varies from milliseconds (ms) to seconds.[21] At the interface, the pure electronic charge transfer via the CB channel occurs on the femtosecond or sub-ps time scale, and the lattice-coupled one via the SB channel on the ps or sub-ns time scale. Among these competitive electronic processes, the fastest one will dominate the apparent interfacial charge transfer.

The essence of the new model and relation is demonstrated here by the comparative studies of anatase and ruitle. First, we clarify the unlike nature of anatase and rutile. Through examining and comparing the characteristic properties including effective masses of CB electron and current carrier, drift and Hall mobilities, and infrared-absorption spectra, we evidence in Appendix A that anatase is rigid ionlike while rutile is small polaronlike. Furthermore, we find that the dramatic difference between anatase and rutile
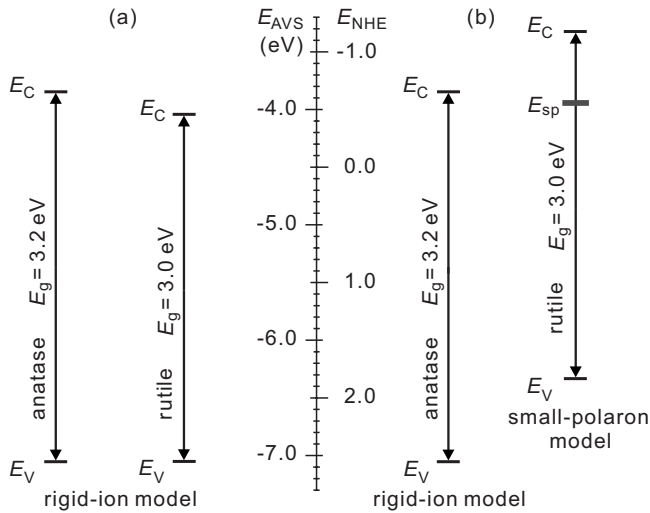
FIG. 2. (a) Standard (Ref. 15) and (b) reassigned band-edge positions of TiO_2 vs the absolute vacuum scale (E_{AVS}) or normal hydrogen electrode scale (E_{NHE}) at pH 7. Rigid-ion model is used in (a) for anatase and rutile and small-polaron model in (b) for rutile. The position of E_{sp} is shown in (b) for rutile.

lies in their distinct lattice anharmonicities, based on detailed analyses of static dielectric constants, infrared-active and Raman-active modes, and electron and nuclear densities. It is the strong electron-multiphonon couplings underlying the large lattice anharmonicities that result in the formation of small polarons in rutile. The detailed procedure is given in Appendix B. Thus, anatase and rutile should be described by rigid-ion model and small-polaron model, respectively.

The BEP of rutile is reassigned in Fig. 2(b), and compared with the standard one in Fig. 2(a). The BEP of anatase is taken as reference. Here, we take the measured E_{fb} for anatase and rutile[15] and $E_b = 0.4$ eV for rutile,[3,4] and estimate $E_{dis} = 0.2$ eV for rutile,[22] $\Delta E = 0.2$ eV and $\Delta E' = 0.3$ eV. The

reassigned E_C of rutile is 0.7 eV higher than its standard value, inverting the relative positions of E_C between anatase and rutile.

Using the reassigned BEP of rutile, we eliminate the aforementioned dilemma of charge transfer in mixed-phase TiO_2 for photocatalysis. As shown in Fig. 3(a), UV light generates electron-hole pairs in both indirect-gap anatase and direct-gap rutile. At the anatase-rutile interface, the electron transfer via the CB-to-CB channel overwhelms the one via the CB-to-SB channel. Thus, the apparent photoinduced electron transfer is from rutile to anatase, in agreement with the experiments.[14]

We revisit the electron-injection processes of TiO_2-based DSSCs in which Ru complex dye N719 is usually used to absorb visible light. Compared to anatase-based DSSC,[10] the less studied rutile-based DSSC has a 30%-reduced short-circuit photocurrent and a one-order-of-magnitude lower electron diffusion coefficient.[23] As shown in Fig. 3(b), electron injection is via the lowest unoccupied molecular orbital (LUMO)-to-CB channel at the anatase-dye interface but via the LUMO-to-SB channel at the rutile-dye interface. The LUMO-to-CB channel is thermodynamically forbidden in the latter case. In the absence of hot-electron injection, the electron-injection time scale in rutile-based DSSC is predicted to be sub-ns, orders of magnitude longer than that of sub-ps measured in anatase-based DSSC.[24] Besides the less amount of adsorbed dye,[23] the slower electron injection may also reduce short-circuit photocurrent in rutile-based DSSC. Additionally, the drift mobility of small polarons in rutile is an order of magnitude smaller than that of electrons in anatase (see Table I in Appendix A). So the distinct electron diffusion coefficients in anatase- and rutile-based DSSCs should be related mainly to differences between anatase and rutile in intrinsic carrier mobilities rather than in the proposed extrinsic origins of density of surface states or interparticle connectivity.[23]
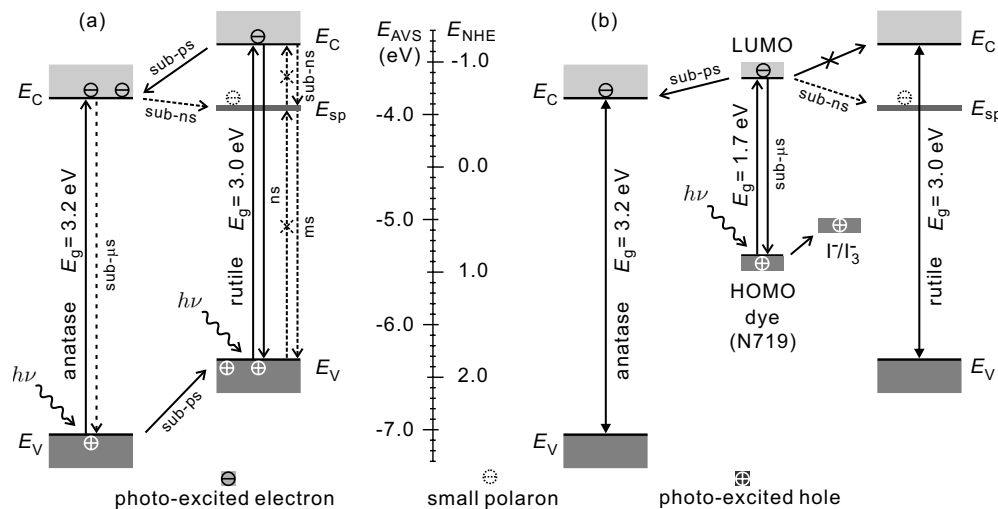
FIG. 3. Schematic of photoinduced electronic processes (a) at the anatase-rutile interface and (b) at the anatase-dye and rutile-dye interfaces. The solid, dashed, and short dashed lines with arrows denote pure, phonon-assisted, and small-polaron-involved electronic processes, respectively. HOMO stands for the highest occupied molecular-orbital level and LUMO the lowest unoccupied molecular-orbital level. The typical time scales are shown for main electronic processes.

TABLE I. Comparison between single-crystal anatase and rutile TiO_2 in the calculated effective mass m^* of CB-bottom electron, the measured effective mass m^{**} of current carrier, drift mobility μ_D, and Hall mobility μ_H (in cm^2/V s), the ratio of μ_H/μ_D, and the wavelength-dependent near infrared absorption (NIA) spectra. m_e denotes the free-electron mass and W_H the thermal activation energy for small-polaron hopping.

TiO_2	Anatase	Rutile
m^*/m_e	~ 1 [a]	~ 1 [b]
m^{**}/m_e	~ 1 [c]	~ 20–150 [d]
μ_D	~ 10–40 [e]	$\propto T^{-1} \exp(-W_H/k_B T)$,[f] ~ 0.1–1 [g]
μ_H	$\propto T^{3/2}$,[h] $\propto T^{-3/2}$,[i] ~ 20 [e]	$\propto T^{-1/2} \exp(-W_H/3k_B T)$,[f] ~ 0.1–1 [g]
μ_H/μ_D	~ 1 [j]	~ 0.01–100 [k]
NIA	No peak[l]	One broad peak[d]
Characteristic	Rigid ionlike	Small polaronlike

[a]Reference 27.
[b]Reference 28.
[c]Reference 30; in thin-film samples of anatase.
[d]References 3 and 4.
[e]At room temperature, according to Ref. 31.
[f]$T > \frac{1}{2}\theta_D \sim 300$ K, θ_D is the Debye temperature (Refs. 3–5).
[g]At room temperature, according to Refs. 3 and 4.
[h]A good fit to the measured low-temperature μ_H (Ref. 31), dominated by impurity scattering.
[i]A good fit to the measured high-temperature μ_H (Refs. 30 and 31), dominated by phonon scattering.
[j]Dependent weakly on temperature (Ref. 4).
[k]Dependent strongly on temperature (Refs. 3–5).
[l]Reference 32; in thin-film samples of anatase.

III. SUMMARY

In summary, we re-examined the models for electronic elementary excitation spectra of semiconductors, and derived an effective relation between the energy-band edge and the Fermi level based on small-polaron model. We showed that the derived relation could be used in electrochemistry to obtain valid BEPs of small-polaron semiconductors, and gained both thermodynamic and kinetic insights into interfacial charge-transfer processes. We identified that anatase is rigid ionlike while rutile is small polaronlike, reassigned the BEP of rutile, eliminated the charge-transfer dilemma in mixed-phase TiO_2, and predicted that electron injection is on the sub-ns time scale in rutile-based DSSC. The prediction calls for experimental verification.

APPENDIX A: RIGID-IONLIKE ANATASE VERSUS SMALL-POLARONLIKE RUTILE

As is known, small-polaron semiconductors are distinct from common or rigid-ionlike semiconductors in many characteristic properties, e.g., effective mass of current carrier, drift and Hall mobilities, and infrared-absorption spectra.[3–5] These characteristic properties can be used as fingerprints to distinguish small-polaron semiconductors from rigid ion ones.

To gain an insight into the rigid-ionlike or small-polaronlike nature of the electronic elementary excitation spectrum for anatase and rutile TiO_2, we examine the above-mentioned characteristic properties based on calculations and measurements in the literature, and draw an interesting comparison between anatase and rutile TiO_2 in Table I.

1. Calculated effective mass of CB electron

In rigid-ion model the majority carriers of a nondegenerate n-type semiconductor are electrons that are thermally excited into the CB bottom. The effective mass m^* of CB-bottom electron of a semiconductor can be derived from the calculated energy-band structure via $m^* = \hbar^2 / \frac{\partial^2 E(k)}{\partial k^2}$, where $\hbar$ is the reduced Planck's constant, E the energy of the electron, and k the wave vector of the electron.[2]

In small-polaron model there is an additional small-polaron band below the common CB. The width of small-polaron band is significantly narrower than that of CB, so the effective mass of small polarons which take the place of electrons as current carriers would be much larger than m^*.[3–5]

It is worthy of note that current computational methods for electronic structure, e.g., density-functional theory (DFT), are based on the Born-Oppenheimer approximation.[25] In other words, nuclei are hold rigidly when solving the Hamiltonian for the system of electrons and nuclei. Since electrons are not considered to displace nuclei, these computational methods can only predict one of the two stable states

in three-dimensional small-polaron semiconductors,[5,16] i.e., the CB electron state. The other stable state, namely, the small-polaron state, corresponding to a strong short-range lattice distortion, cannot be simply reproduced by these computational methods unless nuclei are allowed to relax.[26] Therefore, the electronic structure calculated in the framework of standard DFT is just a rigid-ionlike description of the semiconductor.

For anatase and rutile, standard DFT calculations predict that they have similar energy-band structures and that m^* is close to the free-electron mass m_e within local-density approximation.[27–29] Thus, if rigid-ion model is applicable to TiO$_2$, the measured effective mass of current carrier would be $\sim 1 m_e$ for either anatase or rutile.

2. Measured effective mass of current carrier

The effective mass m^{**} of current carrier for anatase has been estimated $\sim 1 m_e$ in thin-film samples.[30] To the best of our knowledge, there is as yet no reported m^{**} in single-crystal anatase.

In contrast, the m^{**} for rutile, ranging from 20 to $150 m_e$, has been extensively studied in single-crystal samples through experiments such as electrical, optical, and ESR measurements.[3,4]

Apparently, $m^{**} \simeq m^*$ indicates that anatase is rigid ionlike, and $m^{**} \gg m^*$ suggests that rutile is small polaronlike.

3. Measured drift and Hall mobilities

In rigid-ion model the drift mobility μ_D is close to the Hall mobility μ_H. For a typical semiconductor, the low-temperature $\mu_D(\mu_H)$ is dominated by impurity scattering and proportional to $T^{3/2}$, and the high-temperature $\mu_D(\mu_H)$ dominated by acoustic phonon scattering and proportional to $T^{-3/2}$.[2]

In small-polaron model μ_D and μ_H which are both associated with small-polaron hopping differ greatly from each other.[3] In adiabatic approximation μ_D varies as $T^{-1} \exp(-W_H/k_B T)$ while $\mu_H \propto T^{-1/2} \exp(-W_H/3k_B T)$ when $T > \theta_D/2$. Here, W_H denotes the thermal activation energy for small-polaron hopping and θ_D the Debye temperature of the semiconductor.

It should be noted that, compared with $\mu_D(\mu_H)$ of a common semiconductor, $\mu_D(\mu_H)$ of a small-polaron one has a thermally activated feature and would be considerably smaller in magnitude above the temperature $\theta_D/2$.

It is known that the measured temperature-dependent electrical resistivity ρ of single-crystal anatase is similar to that of a conventional semiconductor,[31] indicating that μ_D of anatase behaves normally. From the measured value of room-temperature ρ,[31] we estimate μ_D via $\mu_D = 1/qn\rho$, where q is the elementary charge and n the density of current carriers. The room-temperature μ_D of anatase is estimated ~ 10–40 cm^2/V s.

The temperature-dependent μ_H of anatase has been measured in the single-crystal sample.[31] The μ_H of anatase is ~ 20 cm^2/V s at room temperature. We find that the low-temperature and high-temperature μ_H can be well fitted by

the $T^{3/2}$ and $T^{-3/2}$ laws, respectively. In addition, the high-temperature μ_H of thin-film anatase also follows the $T^{-3/2}$ law.[30]

The μ_D and μ_H of rutile have been well studied in single-crystal samples.[3,4] The room-temperature μ_D and μ_H of rutile were measured ~ 0.1–1 cm^2/V s. In particular, both μ_D and μ_H of rutile show the expected thermally activated feature, and the ratio of μ_H/μ_D, ranging from 0.01 to 100, depends strongly on temperature. The distinct difference in μ_D and μ_H between anatase and rutile indicates that anatase is rigid ionlike while rutile is small polaronlike.

4. Measured near infrared-absorption spectra

For a common semiconductor with a large band gap, the intraband absorption of free-carrier type plays an important role in the mid- and near infrared regions. The absorption coefficient α monotonically increases in proportion to λ^p, where λ is the wavelength of infrared light, and $p = \frac{3}{2}$ and $\frac{5}{2}$ for acoustic and optical phonon scattering, respectively.[17]

For a small-polaron semiconductor, the small-polaron absorption dominates in the near infrared region, and α varies as $\frac{1}{\hbar\omega\Delta}\exp[-\frac{(2E_b-\hbar\omega)^2}{\Delta^2}]$, where ω is the angular frequency of infrared light, Δ the characteristic energy associated with phonon broadening, and E_b the binding energy of small polaron.[8] It should be noted that the small-polaron absorption is characterized by the broad peak around $2E_b$.

To the best of our knowledge, the near infrared-absorption spectra of anatase have only been obtained in thin-film samples.[32] We find that the measured α, which monotonically increases with increasing λ in the wavelength range of ~ 1000–2000 nm, can be well fitted by the λ^p law, where $p \sim 2.0$–2.3 for different samples of anatase in Ref. [32]. The deviation of p from $\frac{3}{2}$ or $\frac{5}{2}$ might be related to the thin-film feature of the samples.

In contrast, the near infrared-absorption spectra of rutile have been well studied in single-crystal samples.[3,4] The measured α exhibits a characteristic broad peak around 6600 cm^{-1} in the 2000–$12\,000$ cm^{-1} frequency range, which is definitely ascribed to the small-polaron absorption.

Again, the measured near infrared-absorption spectra confirm that anatase is rigid ionlike while rutile is small polaronlike.

APPENDIX B: LATTICE ANHARMONICITIES IN ANATASE AND RUTILE

After examining and comparing the characteristic properties, we have indubitably identified the nature of electronic elementary excitation spectra of anatase and rutile TiO$_2$. But why anatase is rigid ionlike while rutile is small polaronlike?

The answer lies in the lattice anharmonicity which is weak in anatase but surprisingly strong in rutile. The distinction in anharmonic effects between anatase and rutile is manifested in many physical properties such as static dielectric constants, infrared-active and Raman-active modes, and electron and nuclear densities.
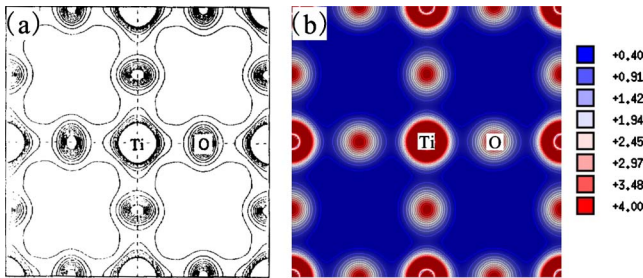
FIG. 4. (Color online) The (a) measured (Ref. 40) and (b) calculated (Ref. 42) electron-density distribution maps of anatase (001) plane which contains the Ti atom. The electron-density region is shown from 0.4 to 4.0 $e\text{Å}^{-3}$.

FIG. 5. (Color online) The (a) measured (Ref. 39) and (b) calculated (Ref. 42) electron-density distribution maps of rutile (002) plane. The electron-density region is shown from 0.4 to 5.0 $e\text{Å}^{-3}$.

1. Dielectric constants and infrared-active modes

The static dielectric constant ϵ_0 of an insulator is related to the infrared-active modes via the Lyddane-Sachs-Teller relation.[33] To the best of our knowledge, there is no report on the temperature dependence of ϵ_0 or infrared modes for anatase. However, the measured room temperature $\epsilon_0 \sim 30$ implies that anatase is somewhat a common dielectric.[34] In contrast, rutile is known as a typical incipient ferroelectric with a large room temperature $\epsilon_0 \sim 167$ and low temperature $\epsilon_0 \sim 251$.[35] For rutile, it is the softening of low-frequency infrared-active modes that gives rise to the dramatic increase in ϵ_0 with decreasing temperature.[35]

The soft modes are associated with lattice instability and anharmonicity.[33,35] So the lattice of rutile would be much more easily distorted than that of anatase.

2. Raman-active modes

As predicted by group theory, anatase has six Raman-active modes $(A_{1g}+2B_{1g}+3E_g)$ due to first-order scattering. These one-phonon Raman-active modes can well explain the measured Raman spectra of anatase.[36] It should be mentioned that, although the temperature dependence of Raman spectra demands a thorough understanding of anharmonicity, there are no noticeable two-phonon Raman peaks due to second-order scattering in the measured Raman spectra of anatase.[36]

In contrast, considering first-order scattering, rutile has four symmetry-allowed Raman-active modes $(1A_{1g}+1B_{1g}+1B_{2g}+1E_g)$. However, the four one-phonon modes cannot fully explain the measured Raman spectra of rutile. There is an extra broad Raman peak ranging from ~ 190 to 280 cm^{-1} in the measured Raman spectra.[37] This extra peak is as strong as the other four peaks, and has been explicitly ascribed to several two-phonon Raman modes due to second-order scattering.[37]

In anharmonic crystals, light or neutrons may interact with two or more phonons simultaneously besides the interaction with single phonons.[38] The multiphonon processes, e.g., in Raman scattering, arise from the nonlinearity in the distortion of the ions.[38] Thus, the novel two-phonon feature of Raman spectra of rutile indicates that a strong nonlinear distortion of ions in rutile can happen when the ions are displaced by particles such as light, neutrons, or excess electrons. In addition, the lack of notable multiphonon feature of Raman spectra implies that the nonlinear distortion of ions would be rather weak in anatase.
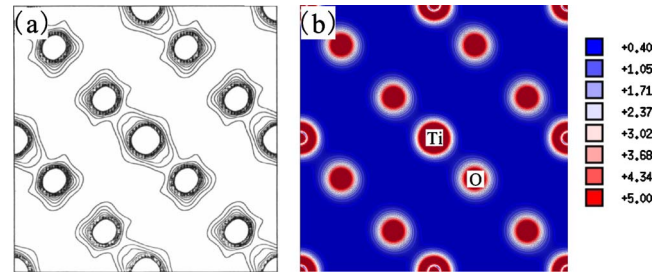
3. Electron and nuclear densities

High-revolution electron and nuclear density distributions of anatase and rutile have been determined by the maximum-entropy method from powder x-ray diffraction data and neutron-diffraction data, respectively.[39–41] Due to anharmonic thermal vibration, there might be skewness in the measured electron and nuclear density distributions.[39] For anatase, there is no notable skewness in electron and nuclear density distributions,[40] as evidenced by the good agreement between the measured and the calculated electron-density distribution maps in Fig. 4. For rutile, however, the oxygen electrons and nuclei are both skewed significantly.[39,41] The poor agreement between the measured and the calculated electron-density distribution maps in Fig. 5 indicates that anharmonic thermal vibration does skew seriously the electron density of rutile.

Thus, the anharmonic thermal vibration is weak in anatase but rather strong in rutile.

We now understand why anatase is rigid ionlike while rutile is small polaronlike. For anatase, the weak electron-multiphonon (anharmonic electron-phonon) couplings cannot compensate the energy required for the strong local lattice distortion. Thus, there is no small-polaron formation in anatase. For rutile, the strong electron-multiphonon couplings can afford the energy required for the strong local lattice distortion. So the excess electrons in the CB state would like to decay into small polarons in rutile.

*liguoling@dicp.ac.cn

†wxli@dicp.ac.cn

‡canli@dicp.ac.cn

[1] P. W. Anderson, *Concepts in Solids: Lectures on the Theory of Solids* (Addison-Wesley, New York, 1992).

[2] C. Kittel, *Introduction to Solid State Physics*, 2nd ed. (Wiley, New York, 1956).

[3] I. G. Austin and N. F. Mott, Adv. Phys. **18**, 41 (1969).

[4] V. N. Bogomolov, E. K. Kudinov, and Y. A. Firsov, Fiz. Tverd. Tela (Leningrad) **9**, 3175 (1967) [Sov. Phys. Solid State **9**, 2502 (1968)]; V. N. Bogomolov and D. N. Mirlin, Phys. Status Solidi **27**, 443 (1968); V. N. Bogomolov, Yu. A. Firsov, K. Kudinov, and D. N. Mirlin, *ibid.* **35**, 555 (1969).

[5] J. T. Devreese, in *Encyclopedia of Applied Physics*, edited by G. L. Trigg (Wiley-VCH, Weinheim, 1996), Vol. 14, p. 383; T. K. Mitra, A. Chatterjee, and S. Mukhopadhyay, Phys. Rep. **153**, 91 (1987).

[6] A. J. Bosman and H. J. Van Daal, Adv. Phys. **19**, 1 (1970).

[7] A. J. Fisher, W. Hayes, and D. S. Wallace, J. Phys.: Condens. Matter **1**, 5567 (1989); O. F. Schirmer, *ibid.* **18**, R667 (2006).

[8] D. Emin, Phys. Rev. B **48**, 13691 (1993).

[9] H. Gerischer, in *Solar Power and Fuels*, edited by J. R. Bolton (Academic, New York, 1977); L. A. Harris and R. H. Wilson, Annu. Rev. Mater. Sci. **8**, 99 (1978); S. R. Morrison, *Electrochemistry at Semiconductor and Oxidized Metal Electrodes* (Plenum, New York, 1980); M. Radecka, M. Rekas, and K. Zakrzewska, Trends Inorg. Chem. **9**, 81 (2006).

[10] B. O'Regan and M. Grätzel, Nature (London) **353**, 737 (1991); K. Hara and H. Arakawa, in *Handbook of Photovoltaic Science and Engineering*, edited by A. Luque and S. Hegedus (Wiley, Chichester, 2003).

[11] M. Grätzel, Nature (London) **414**, 338 (2001).

[12] N. A. Deskins and M. Dupuis, Phys. Rev. B **75**, 195212 (2007); J. Phys. Chem. C **113**, 346 (2009); B. J. Morgan, D. O. Scanlon, and G. W. Watson, J. Mater. Chem. **19**, 5175 (2009).

[13] T. Kawahara, Y. Konishi, H. Tada, N. Thoge, J. Nishii, and S. Ito, Angew. Chem., Int. Ed. **41**, 2811 (2002); J. Zhang, Q. Xu, Z. Feng, M. Li, and C. Li, *ibid.* **47**, 1766 (2008).

[14] T. Ohno, K. Tokieda, S. Higashida, and M. Matsumura, Appl. Catal. A Gen. **244**, 383 (2003); D. C. Hurum, A. G. Agrios, and K. A. Gray, J. Phys. Chem. B **107**, 4545 (2003); G. Li and K. A. Gray, Chem. Phys. **339**, 173 (2007).

[15] J. M. Bolts and M. S. Wrighton, J. Phys. Chem. **80**, 2641 (1976); M. V. Rao, K. Rajeshwar, V. R. P. Verneker, and J. DuBow, *ibid.* **84**, 1987 (1980); L. Kavan, M. Grätzel, S. E. Gilbert, C. Klemenz, and H. J. Scheel, J. Am. Chem. Soc. **118**, 6716 (1996); A. Mills and S. Le Hunte, J. Photochem. Photobiol., A **108**, 1 (1997).

[16] D. Emin and T. Holstein, Phys. Rev. Lett. **36**, 323 (1976).

[17] P. K. Basu, *Theory of Optical Processes in Semiconductors* (Oxford, New York, 1997); A. J. Nozik, Annu. Rev. Phys. Chem. **52**, 193 (2001); S. K. Sundaram and E. Mazur, Nature Mater. **1**, 217 (2002); R. F. Haglund, Jr., in *3D Laser Microfabrication*, edited by H. Misawa and S. Juodkazis (Wiley-VCH, Weinheim, 2006).

[18] T. Holstein, Ann. Phys. (N.Y.) **8**, 343 (1959); N. F. Mott and A. M. Stoneham, J. Phys. C **10**, 3391 (1977); A. A. Johansson and S. Stafström, Phys. Rev. B **69**, 235205 (2004).

[19] For interband transition, the contribution from E_V to E_{sp} is many orders of magnitude smaller than that from E_V to E_C, D. M.

Eagles, Phys. Rev. B **130**, 1381 (1963).

[20] J. L. Bredas and G. B. Street, Acc. Chem. Res. **18**, 309 (1985).

[21] H. Guenther, R. Macfarlane, Y. Furukawa, K. Kitamura, and R. Neurgaonkar, Appl. Opt. **37**, 7611 (1998).

[22] E_{dis} is presently unknown. Fortunately, the value of E_{dis} for rutile does not qualitatively alter the relative energy-level positions between rutile and anatase or dye N719.

[23] N.-G. Park, J. van de Lagemaat, and A. J. Frank, J. Phys. Chem. B **104**, 8989 (2000).

[24] M. Hilgendorff and V. Sundström, J. Phys. Chem. B **102**, 10505 (1998); D. F. Watson and G. J. Meyer, Annu. Rev. Phys. Chem. **56**, 119 (2005); W. R. Duncan and O. V. Prezhdo, *ibid.* **58**, 143 (2007).

[25] R. M. Martin, *Electronic Structure: Basic Theory and Practical Methods* (Cambridge University Press, Cambridge, 2004).

[26] Even if nuclei are allowed to relax, standard DFT is known incapable of modeling small polarons in real materials. *Beyond* DFT methods, e.g., DFT+U and hybrid DFT, have recently been employed to model small polarons, Ref. 12; S. Lany and A. Zunger, Phys. Rev. B **80**, 085202 (2009); A. Droghetti, C. D. Pemmaraju, and S. Sanvito, *ibid.* **81**, 092403 (2010); W. R. L. Lambrecht, Phys. Status Solidi B (to be published); in particular, DFT+U calculations predict that anatase and rutile have similar localized "small-polaron" states within the band gap (Ref. 12). However, according to experimental data in the literature, we can safely say that anatase does not have any fingerprints of small polarons. Therefore, there must be something wrong with DFT+U calculations in modeling small polarons, and DFT+U calculations cannot tell the dramatic difference between anatase and rutile. Based on comparative calculations, we will show in our forthcoming paper why beyond DFT methods fail in modeling small polarons, G.-L. Li, H. Jiang, and W.-X. Li (unpublished).

[27] X. D. Liu, E. Y. Jiang, Z. Q. Li, and Q. G. Song, Appl. Phys. Lett. **92**, 252104 (2008).

[28] C. Persson and A. F. da Silva, Appl. Phys. Lett. **86**, 231912 (2005).

[29] Strictly speaking, the effective mass m^* is a tensor. For either anatase or rutile, the anisotropic m^* has two independent components $m_\parallel^*$ (m^* in the c direction) and $m_\perp^*$ which are comparable in magnitude.

[30] H. Tang, K. Prasad, R. Sanjinès, P. E. Schmid, and F. Lévy, J. Appl. Phys. **75**, 2042 (1994).

[31] L. Forro, O. Chauvet, D. Emin, L. Zuppiroli, H. Berger, and F. Lévy, J. Appl. Phys. **75**, 633 (1994).

[32] N. Yamada, T. Hitosugi, N. L. H. Hoang, Y. Furubayashi, Y. Hirose, S. Konuma, T. Shimada, and T. Hasegawa, Thin Solid Films **516**, 5754 (2008).

[33] F. Gervais and W. Kress, Phys. Rev. B **28**, 2962 (1983).

[34] R. J. Gonzalez, R. Zallen, and H. Berger, Phys. Rev. B **55**, 7014 (1997).

[35] G. A. Samara and P. S. Peercy, Phys. Rev. B **7**, 1131 (1973).

[36] T. Ohsaka, J. Phys. Soc. Jpn. **48**, 1661 (1980); D. Wang, B. Chen, and J. Zhao, J. Appl. Phys. **101**, 113501 (2007); M. Mikami, S. Nakamura, O. Kitao, and H. Arakawa, Phys. Rev. B **66**, 155213 (2002).

[37] S. P. S. Porto, P. A. Fleury, and T. C. Damen, Phys. Rev. **154**, 522 (1967); J. H. Nicola, C. A. Brunharoto, M. Abramovich, and C. E. T. Conçalves da Silva, J. Raman Spectrosc. **8**, 32 (1979).

[38] R. A. Cowley, Rep. Prog. Phys. **31**, 123 (1968).

[39] M. Sakata, T. Uno, M. Takata, and R. Mori, Acta Crystallogr., Sect. B: Struct. Sci. **48**, 591 (1992).

[40] M. Sakata, M. Takagi, M. Takata, and C. J. Howard, Physica B **213–214**, 384 (1995).

[41] M. Sakata, T. Uno, and M. Takata, J. Appl. Crystallogr. **26**, 159 (1993); S. Kumazawa, M. Takata, and M. Sakata, Acta Crystallogr., Sect. A: Found. Crystallogr. **51**, 651 (1995).

[42] We calculate the zero-temperature valence electron densities of anatase and rutile using the full-potential linearized augmented plane-wave method within the Perdew-Burke-Ernzerhof (PBE) generalized-gradient approximation for the exchange-correlation energy via the DFT code WIEN2K, P. Blaha, K. Schwarz, G. K. H. Madsen, D. Kvasnicka, and J. Luitz, *WIEN2k: An Augmented PlaneWave + Local Orbitals Program for Calculating Crystal Properties* (Techn. Universität Wien, Austria, 2009); the experimental lattice parameters of anatase and rutile, C. J. Howard, T. M. Sabine, and F. Dickson, Acta Crystallogr., Sect. B: Struct. Sci. **47**, 462 (1991) are taken in the calculations. The muffin-tin sphere radii are 1.94 a.u. for Ti and 1.72 a.u. for O. To compare with the measured valence electron densities, the Ti $1s^2 2s^2 2p^6$ orbitals are treated as core states, and all the others as valence states. The cutoff parameter takes $RK_{max} = 7.0$. And self-consistent calculations are carried out on a 126 (280) k-point mesh for anatase (rutile) in the irreducible Brillouin zone.